International Journal of Nanomedicine

Dovepress
open access to scientific and medical research

Open Access Full Text Article

ORIGINAL RESEARCH

Effect of intratumoral administration on biodistribution of ^{64}Cu-labeled nanoshells

This article was published in the following Dove Press journal:
International Journal of Nanomedicine
2 May 2012
Number of times this article has been viewed

Huan Xie[1]
Beth Goins[2]
Ande Bao[2]
Zheng Jim Wang[3]
William T Phillips[2]

[1]Department of Pharmaceutical Sciences, College of Pharmacy and Health Sciences, Texas Southern University, Houston, TX, [2]Department of Radiology, University of Texas Health Science Center at San Antonio, San Antonio, TX, [3]MPI Research Inc, Mattawan, MI, USA

Video abstract

Point your SmartPhone at the code above. If you have a QR code reader the video abstract will appear. Or use: http://bit.ly/HMneRj

Correspondence: Huan Xie
Texas Southern University,
3100 Cleburne Street, Gray Hall 119,
Houston, TX 77004, USA
Tel +1 71 3313 4340
Fax +1 71 3313 1091
Email xieh@tsu.edu

Background: Gold nanoshells are excellent agents for photothermal ablation cancer therapy and are currently under clinical trial for solid tumors. Previous studies showed that passive delivery of gold nanoshells through intravenous administration resulted in limited tumor accumulation, which represents a major challenge for this therapy. In this report, the impact of direct intratumoral administration on the pharmacokinetics and biodistribution of the nanoshells was systematically investigated.

Methods: The gold nanoshells were labeled with the radionuclide, copper-64 (^{64}Cu). Intratumoral infusion of ^{64}Cu-nanoshells and two controls, ie, ^{64}Cu-DOTA (1,4,7,10-tetraazaciclododecane-1,4,7,10-tetraacetic acid) and ^{64}Cu-DOTA-PEG (polyethylene glycol), as well as intravenous injection of ^{64}Cu-nanoshells were performed in nude rats, each with a head and neck squamous cell carcinoma xenograft. The pharmacokinetics was determined by radioactive counting of serial blood samples collected from the rats at different time points post-injection. Using positron emission tomography/computed tomography imaging, the in vivo distribution of ^{64}Cu-nanoshells and the controls was monitored at various time points after injection. Organ biodistribution in the rats at 46 hours was analyzed by radioactive counting and compared between the different groups.

Results: The resulting pharmacokinetic curves indicated a similar trend between the intratumorally injected agents, but a significant difference with the intravenously injected ^{64}Cu-nanoshells. Positron emission tomography images and organ biodistribution results on rats after intratumoral administration showed higher retention of ^{64}Cu-nanoshells in tumors and less concentration in other healthy organs, with a significant difference from the controls. It was also found that, compared with intravenous injection, tumor concentrations of ^{64}Cu-nanoshells improved substantially and were stable at 44 hours post-injection.

Conclusion: There was a higher intratumoral retention of ^{64}Cu-nanoshells and a lower concentration in other healthy tissues, suggesting that intratumoral administration is a potentially better approach for nanoshell-based photothermal therapy.

Keywords: gold nanoshells, intratumoral administration, positron emission tomography, biodistribution

Introduction

One of the most promising recent advances in cancer treatment has been thermal ablation, which provides a minimally invasive or noninvasive technique that rapidly kills cancer cells by heat. Among the various thermal ablation methods, gold nanoshell-assisted photothermal ablation, a laser-induced thermal therapy that utilizes the special optical properties of gold nanoshells, offers advantages over traditional thermal

therapies and has already demonstrated effectiveness in the elimination of solid tumors in animal models.[1,2] Clinical investigation of nanoshells in head and neck cancer patients is ongoing. Nanoshells are spherical nanoparticles consisting of a dielectric core and a metal shell, where the plasmon resonance frequency is determined by the relative size of the core and the metal shell layer.[3] By adjusting the relative core and shell thicknesses, nanoshells can be fabricated to absorb or scatter light across the visible and near-infrared regions (700–1300 nm) of the electromagnetic spectrum, where optical transmission through tissue is optimal. They can be manufactured with size ranges (60–400 nm) that can accumulate in tumors via the enhanced permeability and retention effect, which is attributed to the leaky nature of tumor vessels.[4] However, our previous research found that accumulation of nanoshells in solid tumors via the enhanced permeability and retention effect is very limited when they are injected intravenously,[5–7] which hinders the efficacy of subsequent photothermal ablation, and is a major challenge for this therapy.

Direct intratumoral injection of anticancer agents has been extensively evaluated in the past few decades.[8–12] Studies have suggested that intratumoral injection can increase the concentrations of agents at the target site, while decreasing their localization to healthy tissues. However, intratumoral injection has not been established as an alternative route of administration in routine clinical practice. This is probably due to the relatively rapid clearance of the administered drugs from tumors, high toxicities in tissues surrounding the site of application, and availability of other more standardized treatment modalities (eg, surgery and radiotherapy) to the types of tumors (mostly solid tumors and surface tumors) accessible for intratumoral injection.[13] However, these concerns are not necessarily significant for some contemporary cancer agents. For example, there have been many reports of intratumoral injection of different nanocompositions, such as liposomes,[14,15] magnetic cationic liposomes,[16] hyaluronan nanoparticle formulations,[17] N-(2-hydroxypropyl)-methacrylamide copolymer,[13] cisplatin-loaded polycaprolactone polymers,[18] holmium-loaded poly-L-lactide polymers,[19] docetaxel-loaded polycaprolactone polymers,[20] multiwalled carbon nanotubes,[21] gold-dendrimer composite nanodevices,[22] folate-conjugated shell cross-linked nanoparticles,[23] and gum Arabic glycoprotein-functionalized gold nanoparticles.[24] However, intratumoral injection of other newly developed nanoparticles has been rarely reported, although it is theoretically a good route of administration. For example, mesoporous silica nanocomposite systems including gold nanoshells, dye-doped silica nanoparticles, and iron-oxide shell silica core nanoparticles were only studied by intravenous administration.[25] Layer-by-layer-assembled materials have been developed chiefly for either implantation or injection, and the intravenous, intraperitoneal, or subcutaneous injection routes provide different biodistribution profiles, while targeted delivery using specific targeting molecules have also been investigated, but intratumoral administration has not been reported.[26–28] Quantum dots have been investigated extensively by surface conjugation with different targeting moieties so that they can be biocompatible and achieve better delivery to the target sites; again most of the in vivo studies were done intravenously.[29] Von Maltzahn et al reported x-ray computed tomography (CT) images of gold nanorods in animal tumors that were intratumorally injected into mice, but they did not systematically compare the biodistribution of gold nanorods administered by intratumoral and intravenous injection.[30] Recently, Huang et al re-examined active and passive tumor targeting using gold nanorods, and found active molecular targeting of the tumor microenvironment did not significantly influence nanoparticle uptake by the tumor, suggesting intratumoral injection rather than intravenous injection as the preferred route of nanorod administration,[31] although follow-up intratumoral administration studies have not been reported.

Here we report for the first time an investigation of the feasibility of injecting gold nanoshells directly into solid tumors for subsequent near-infrared photothermal therapy. Because this therapy has been mainly used for solid tumors as well as easily accessible surface tumors, to which intratumoral administration is well suited, we chose nude rats with head and neck squamous cell carcinoma (HNSCC) xenografts as our animal model. To investigate the fate of nanoshells after intratumoral administration and compare the outcome with that of intravenous administration, in vivo pharmacokinetics and biodistribution data are required, and can be obtained by labeling gold nanoshells with photon-emitting radionuclides and carrying out multiple assessments using noninvasive imaging techniques in the same animal across different time points. Previously, we have reported a method for radiolabeling gold nanoshells with both copper-64 (^{64}Cu) and indium-111 (^{111}In) through a bifunctional polyethylene glycol (PEG) and 1,4,7,10-tetraazaciclododecane-1,4,7,10-tetraacetic acid (DOTA), a chelating agent.[5–7] Radiolabeling a chelating agent with these agents permits determination of the biodistribution of radiolabeled nanoshells in live rats bearing HNSCC xenografts by noninvasive positron emission

tomography (PET) and single-photon emission computed tomography (SPECT) imaging.[5–7]

The studies reported here were conducted by labeling gold nanoshells with radionuclide ^{64}Cu, using small-animal PET/CT imaging of rats with HNSCC xenografts at various time points after administration, obtaining pharmacokinetic data from the measurement of radioactivity in blood samples, and post-sacrifice tissue counting to determine the distribution of ^{64}Cu-nanoshells. The retention and intratumoral distribution of ^{64}Cu-nanoshells were assessed by both imaging and tissue biodistribution studies, and the results were compared between animals that were intratumorally and intravenously injected with ^{64}Cu-nanoshells to determine the potential benefit of intratumoral injection for gold nanoshell-assisted photothermal ablation cancer therapy. In addition, the in vivo stability of the ^{64}Cu-nanoshell labeling method was indirectly assessed by comparing the tissue biodistribution patterns of ^{64}Cu-nanoshells with those of two separate ^{64}Cu labeling controls, ie, ^{64}Cu-DOTA and ^{64}Cu-DOTA-PEG. Intratumoral administration was demonstrated to improve tumor accumulation of the gold nanoshells significantly up to 44 hours, with excellent stability and lower concentrations in healthy tissue. Our study indicates that intratumoral administration of gold nanoshells could be an ideal method for treating larger solid tumors directly with thermal therapy while minimizing thermal damage to surrounding normal tissues.

Materials and methods

Radiolabeling of nanoshells

The gold nanoshells were synthesized as previously described.[32] Gold nanoshell formation was assessed using an ultraviolet-visible spectrophotometer (U-0080D, Hitachi, Schaumburg, IL) and Zetasizer (Nano-ZS, Malvern, Westborough, MA). Nanoshells manufactured in this manner have an 8–10 nm gold shell around a 110–120 nm silica sphere. The radiolabeling process for the gold nanoshells has been described in our previous publications.[5–7] As Figure 1A shows, a bifunctional chelating agent DOTA-NH_2 (S-2-(4-aminobenzyl)-1, 4, 7, 10-tetraazacyclododecane tetraacetic acid, Macrocyclics, Dallas, TX) was conjugated to bifunctional OPSS-PEG-NHS (opyridyldisulfide-PEG 2000-N-hydroxysuccinimide ester, Nektar, Huntsville, AL). DOTA-NH_2 and OPSS-PEG-NHS were mixed in a 1:1 molar ratio and the mixture was incubated overnight at room temperature. The resulting OPSS-PEG-DOTA was then added to a nanoshell solution (in 10 mM phosphate buffer, pH 7) at a 10,000:1 molar ratio, followed by overnight incubation at room temperature on a shaker, allowing the OPSS group to conjugate with the gold surface of the particles. The mixture was centrifuged and the supernatant with unconjugated OPSS-PEG-DOTA was removed. The pellets of DOTA-gold nanoshells were resuspended in phosphate buffer and checked with the spectrophotometer and Zetasizer to determine the gold nanoshell concentration and size for further conjugation. All the radioactive research was performed at the Department of Radiology, University of Texas Health Science Center at San Antonio. $^{64}CuCl_2$ (Washington University, St Louis, MO) was diluted in 30 mM ammonium citrate buffer (pH 6.5). Next, 213 mBq (5.76 mCi) of ^{64}Cu was added to 450 μL of the DOTA-gold nanoshell solution (about 0.8 nM) followed by the addition of blocking agent PEG5k-SH (Nektar) in a 300,000:1 molar ratio and incubation at room temperature on a shaker for one hour. The mixtures were then centrifuged to remove the unconjugated $^{64}CuCl_2$ and PEG5k-SH. The ^{64}Cu activity of the supernatant and pellet were measured in a dose calibrator (Atomlab 100, Biodex, Shirley, NY). The labeling efficiency of the ^{64}Cu nanoshells was calculated as [activity in pellet/(activity in supernatant + activity in pellet)] × 100, which was 81.3%.

The control samples were ^{64}Cu-DOTA and ^{64}Cu-DOTA-PEG. ^{64}Cu-DOTA was prepared by mixing 74 mBq (2.0 mCi) of $^{64}CuCl_2$ with 200 μL of 0.20 mM DOTA solution (pH 6.5) and incubating at 37°C for 90 minutes. The ^{64}Cu-DOTA-PEG was prepared by mixing 74 mBq (2.0 mCi) of $^{64}CuCl_2$ with 200 μL of 0.20 mM DOTA-PEG solution (pH 6.5) and incubating at 37°C for 90 minutes. Formation of ^{64}Cu complexes were verified by radiothin layer chromatography using a mobile phase consisting of 50:50 MeOH/10% ammonium acetate on silica plates.

Animal model, intratumoral infusion, and image acquisition

A human HNSCC xenograft model in nude rats was established via subcutaneous inoculation of a HNSCC cell line (SCC-4), as reported previously.[33] Animal experiments with radioactive agents were performed at the University of Texas Health Science Center at San Antonio according to the National Institutes of Health animal use guidelines and Institutional Animal Care and Use Committee approval.

All animals were treated 14 days after tumor cell inoculation. On that day, the average weight of the rats was 199.3 ± 17.2 g and the average tumor volume was 1.84 ± 0.61 cm^3. During each animal handling procedure, the animals were anesthetized by inhalation of 1%–3% isoflurane (Vedco, Saint Joseph, MO) in 100% oxygen with

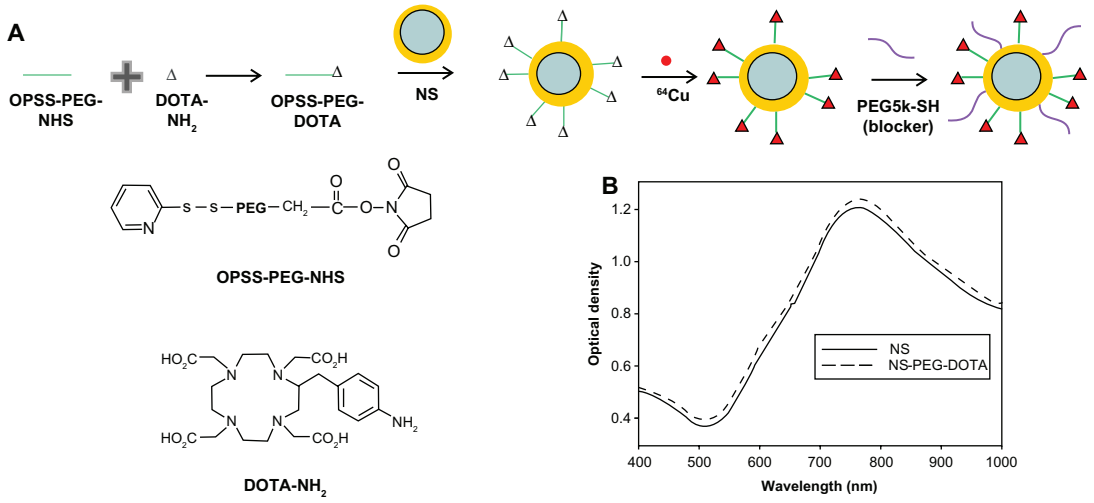

Figure 1 (**A**) Radiolabeling scheme of gold nanoshells with ^{64}Cu through bifunctional OPSS-PEG-NHS and DOTA-NH$_2$. (**B**) Ultraviolet-visible spectra of gold nanoshells before and after conjugation with OPSS-PEG-DOTA.

Abbreviations: PEG, polyethylene glycol; DOTA, 1,4,7,10-tetraazaciclododecane-1,4,7,10-tetraacetic acid; NS, gold nanoshells; NHS, hydroxysuccinimide ester; OPSS, opyridyldisulfide.

use of a veterinary inhalant anesthesia machine (Bickford, Wales Center, NY). Three groups of rats were intratumorally treated, with two controls, ie, ^{64}Cu-DOTA (n = 3, group 1) and ^{64}Cu-DOTA-PEG (n = 3, group 2) as well as ^{64}Cu-NS (n = 4, group 3), respectively. For all the above groups, the tumors were infused with an infusion pump (KD Scientific, Holliston, MA) to deliver the assigned therapy volume and radioactivity. The rate of infusion was 0.5 mL/minute. The radioactivity of the infusion solutions was 577, 528, and 600 μCi/mL for groups 1, 2, and 3, respectively. A 23-gauge needle attached to an infusion pump by polyethylene tubing was inserted into the tumor as guided by direct visual placement and palpation. The total infusion volume for each rat tumor was 30% of the tumor volume from caliper measurements determined on the day of the study. To achieve better tumor coverage, each animal received a series of three percutaneous injections (10% of total tumor volume with each injection) with a 15-minute gap between each consecutive injection. The needle placements for each injection were equally spaced along the largest central section area of the tumor, with each needle tip at approximately one third depth in the tumor along the needle insertion direction.

A separate control group of nude rats bearing HNSCC tumors (n = 4, group 4) was intravenously injected with ^{64}Cu-nanoshells (0.5 mL of 460–490 μCi of ^{64}Cu activity) into the tail vein. The rat tail was large enough to insert a needle in the contralateral vein or in a place well above the injection site for collecting the subsequent blood samples.

One rat from group 1, one rat from group 2, all four rats from group 3, and all four rats from group 4 were selected for PET/CT imaging at hours 1, 4, 20, and 44 post-injection using FLEX X-PET/CT/SPECT (Gamma Medica-Ideas Inc, Northridge, CA) followed by CT image acquisition (80 kVp, 0.25 mA, 256 projections).

Pharmacokinetic and biodistribution studies

Blood samples (40 μL) were collected from the tail veins of the anesthetized nude rats from groups 1 to 4 at 5 minutes and hours 1, 4, 20, and 42 post-injection. ^{64}Cu radioactivity in the blood samples were measured by a gamma-counter (Wallac 1480, Perkin Elmer Life Sciences, Boston, MA). The data are presented as average ± standard deviation from each group. The SigmaPlot 10.0 (Systat Software Inc, San Jose, CA) was used to obtain the curve fitting for the pharmacokinetic data.

After completion of the last imaging session and blood collection, the rats were sacrificed at 46 hours post-injection by cervical dislocation under deep isoflurane anesthesia. The organs of interest were removed and wet-weighed. Radioactivity in the tissues was measured using a gamma counter. The radioactivity of the tissue samples was normalized against a known aliquot of the injectate. The percent injected dose per gram of tissue (%ID/g) values were calculated using the following equation:

$$\%ID/g = \frac{(\text{CPM in sample} - \text{Background}) \times 100}{(\text{Tissue weight}) \times (\text{CPM in standard}) \times \frac{(\text{Injection volume})}{(\text{Standard volume})}}$$

The percent injected dose per organ (%ID/organ) values were calculated using the following equation:

$$\%\text{ID/organ} = \frac{(\text{CPM in sample} - \text{Background}) \times (\text{Correction factor}) \times 100}{(\text{CPM in standard}) \times \frac{(\text{Injection volume})}{(\text{Standard volume})}}$$

Total activity in bone, muscle, and skin was calculated assuming 10%, 40%, and 13% of the rat body weight, respectively.[34,35]

Statistical analysis

All values are expressed as average ± standard deviation. One-way analysis of variance and post hoc multiple comparison (Bonferroni's *t*-test) on the pharmacokinetic and biodistribution data (%ID/g and %ID/organ) were performed using Systat 12 (Systat Software Inc, San Jose, CA). *P* values <0.05 were considered to be statistically significant.

Results

Radiolabeling of nanoshells

Nanoshells used in this study were manufactured to be comprised of a silica core (about 120 nm in diameter) and a gold shell (8–10 nm) to absorb light at the near-infrared region. The ultraviolet-visible spectrum showed the nanoshell peak at about 760 nm (Figure 1B). Zetasizer measurements showed the nanoshell size was around 140 nm in diameter and zeta potential was around −50 mV. A conjugation procedure developed previously[7] was applied to label the nanoshells with ^{64}Cu (elimination half-life 12.7 hours), using bifunctional OPSS-PEG-NHS and the bifunctional chelating agent, DOTA-NH_2 (Figure 1A). First, OPSS-PEG-NHS and DOTA-NH_2 were mixed, and the NHS ester reacted with the amine group to form an amide bond. The mixture was then added to a nanoshell solution, allowing the OPSS group to attach to the gold surface of the particles to obtain gold nanoshell-PEG-DOTA. Ultraviolet-visible spectra show that this intermediate had a peak at 765 nm, slightly shifted to a higher wavelength (Figure 1B), which normally indicates successful conjugation. Gold nanoshell-PEG-DOTA were then coupled with ^{64}Cu through DOTA. Finally, the longer PEG5k-SH was added to block the remaining empty areas on the gold surface to provide better PEG coverage. Zetasizer measurements showed that, after surface modification, the gold nanoshell size increased to about 170 nm in diameter and zeta potential was around −5 mV.

Pharmacokinetics

First, the impact of intratumoral injection on the circulation kinetics of ^{64}Cu-nanoshells and its two controls, ^{64}Cu-DOTA and ^{64}Cu-DOTA-PEG, were investigated in nude rats with human HNSCC xenografts. Blood samples were collected at 5 minutes, and at hours 1, 4, 20, and 42 post-injection for radioactive counting. The simulated exponential decay circulation curves (three-parameter exponential decay model) were obtained for ^{64}Cu-DOTA, ^{64}Cu-DOTA-PEG2 K, and ^{64}Cu-nanoshells based on the average %ID in the blood samples from rats in each group (three rats per group for the two controls and four rats per group for ^{64}Cu-nanoshells) at the same time points (Figure 2A). In general, these three curves have very similar decay, with a higher percentage of ^{64}Cu-nanoshells entering the systemic circulation at 5 minutes post-injection, but there were only small portions of all of these materials left in the blood after one hour. The pharmacokinetic behaviors of these materials are quite different than when intravenously administered, as we have reported previously.[7]

Next, the circulation kinetics of intratumorally administered and intravenously administered ^{64}Cu-nanoshells were compared. As Figure 2B shows, up to 42 hours post-injection, the blood concentrations of intratumorally applied ^{64}Cu-nanoshells were significantly lower than those of intravenously administered ^{64}Cu nanoshells. At one hour and 42 hours post-injection, for example, 22.5% ± 13.6% and 2.3% ± 0.2% ID were found in blood for intratumoral injection, compared with 42.8% ± 6.9% ($P < 0.0001$) and 4.0% ± 1.0% ID ($P = 0.014$, $P < 0.05$) for intravenous injection. This indicates that a large portion of intratumorally injected gold nanoshells are retained in the tumor and only a small percentage entered the systemic circulation. For intravenous injection, gold nanoshells are required to have reasonable stability in the circulation and to avoid recognition by the reticuloendothelial system so that a higher percentage of nanoshells can enter the targeted tumor site. The intravenously injected ^{64}Cu-nanoshells had an average blood clearance half-life of 12.76 hours in the tumor-bearing rats, which is similar to other intravenously injected gold nanoparticles with smaller size.[30,36] The different administration routes leading to the different pharmacokinetic behaviors of ^{64}Cu-nanoshells are shown here.

PET imaging

Using PET/CT imaging, we monitored the in vivo distribution at various time points after intratumoral administration of ^{64}Cu-nanoshells and the two controls as

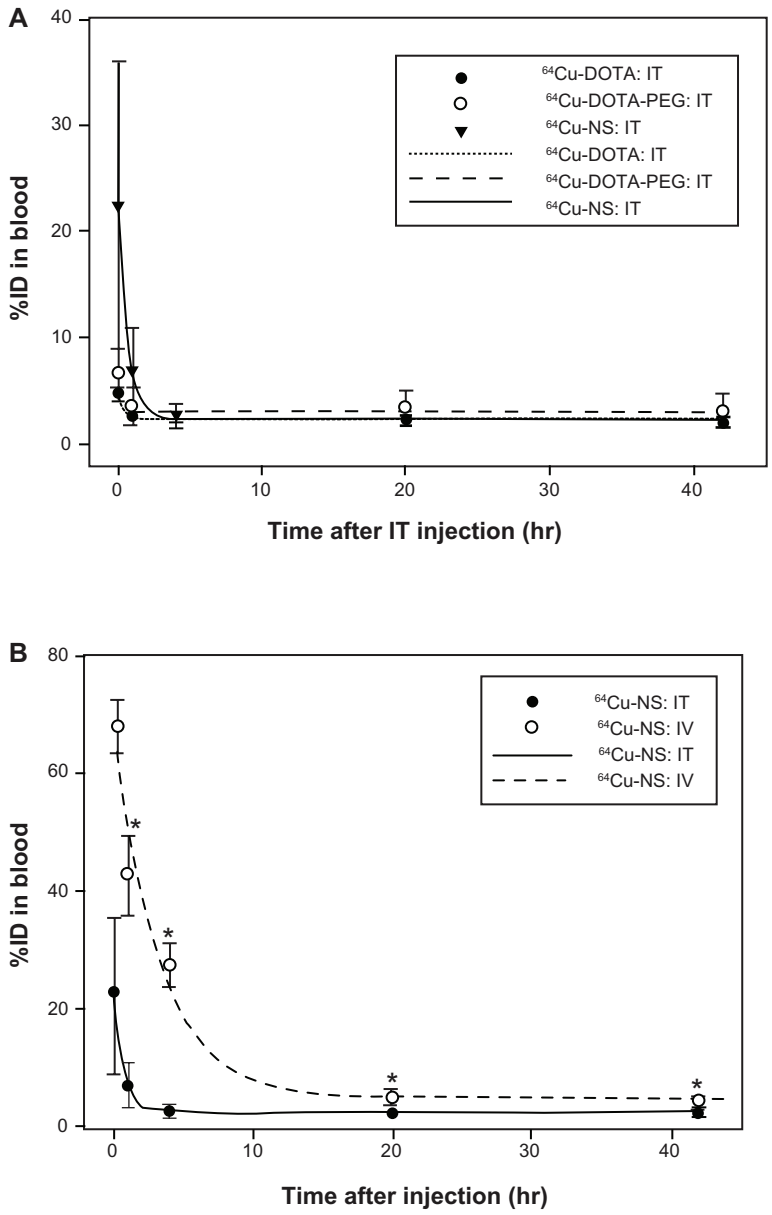

Figure 2 Pharmacokinetics, expressed as a percentage of the injected dose (%ID) in blood, of (**A**) ^{64}Cu-DOTA, ^{64}Cu-DOTA-PEG, and ^{64}Cu-NS at 5 minutes, and at hours 1, 4, 20, and 42 after intratumoral injection, and (**B**) ^{64}Cu-nanoshells administered by intratumoral versus intravenous injection.

Notes: The data points are the average values of three rats for ^{64}Cu-DOTA and ^{64}Cu-DOTA-PEG and the average values of four animals for ^{64}Cu-nanoshells (average ± standard deviation). The curves are the simulated three-parameter single exponential decay. Significant difference between intratumoral and intravenous administration of ^{64}Cu-nanoshells is evident at hours 1, 4, 20, and 42 after injection ($P < 0.05$).

Abbreviations: PEG, polyethylene glycol; DOTA, 1,4,7,10-tetraazaciclododecane-1,4,7,10-tetraacetic acid; NS, gold nanoshells; IT, intratumoral; IV, intravenous.

well as intravenous injection of ^{64}Cu-nanoshells in nude rats with HNSCC xenografts. Figure 3 shows the PET coronal images of three rats at hours 1, 4, 20 and 44 after intratumoral injection of ^{64}Cu-DOTA, ^{64}Cu-DOTA-PEG, and ^{64}Cu-nanoshells, as well as the corresponding CT images denoting the location of the tumor in each rat. As we can see, the amount of the two control substances retained in the tumor decreased slowly over the first 20 hours but became very weak at 44 hours post-injection. Correspondingly, there was some accumulation in the liver and spleen at one hour which declined over time, suggesting that the controls cleared rapidly from the body. This observation agrees with the pharmacokinetic curves shown in Figure 2A. In contrast, the ^{64}Cu-nanoshells maintained high concentrations in the tumor up to 44 hours; uptake to the liver and spleen was consistent in the first 20 hours, and became almost invisible at 44 hours post-injection, which suggests slower clearance than for the two controls, but stable and high tumor retention of gold nanoshells at the end time point. These results also confirm that the radioisotope distribution truly reflected the

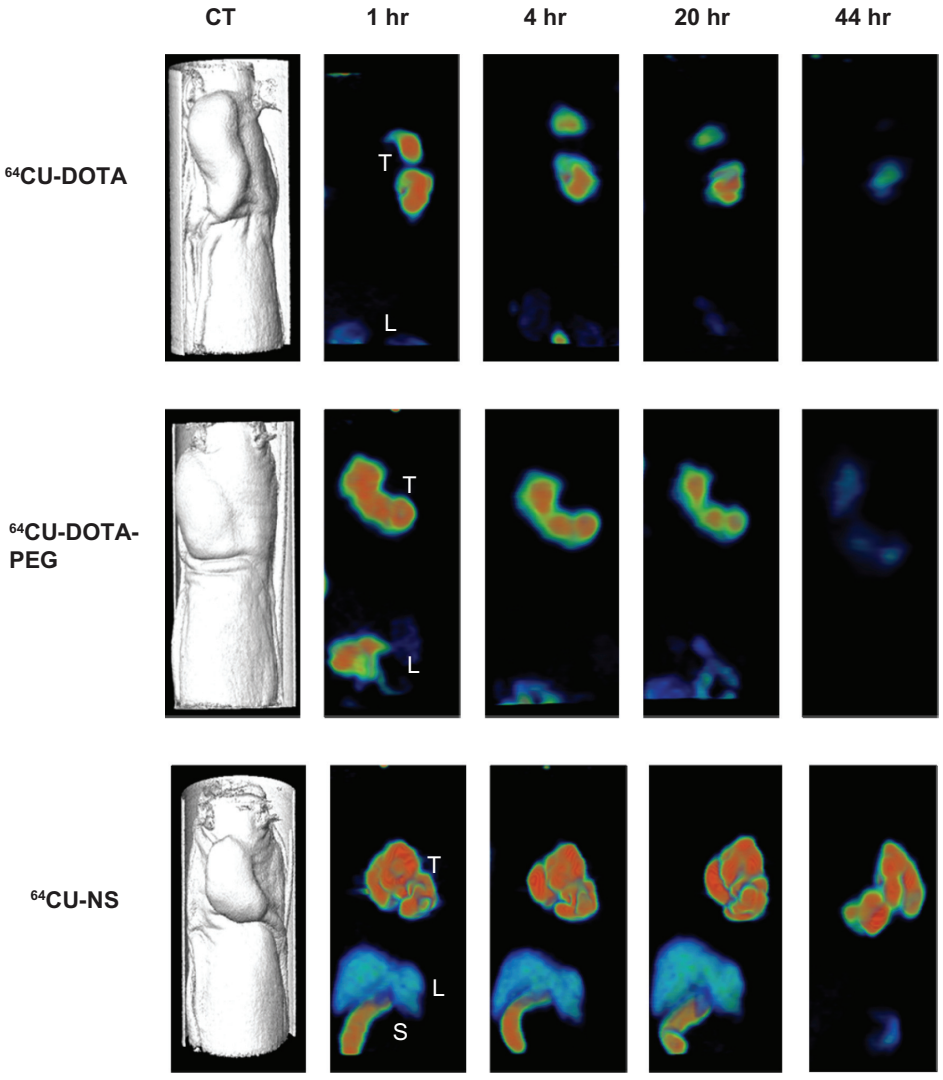

Figure 3 Coronal PET images of three HNSCC xenograft-bearing nude rats acquired at various time points after intratumoral injection of ^{64}Cu-DOTA, ^{64}Cu-DOTA-PEG, and ^{64}Cu-NS, respectively.
Notes: Surface-rendered CT images depicting tumor location are also shown. Color intensity scale is denoted as red > yellow > green > blue.
Abbreviations: L, liver; S, spleen; T, tumor; PEG, polyethylene glycol; DOTA, 1,4,7,10-tetraazaciclododecane-1,4,7,10-tetraacetic acid; NS, gold nanoshells; PET, positron emission tomography; CT, computed tomography; HNSCC, head and neck squamous cell carcinoma.

gold nanoshell distribution because it was quite different from the two other controls, which agrees with our previous report.[7]

PET images showing the tumor localization and organ distribution of intratumorally and intravenously administered gold nanoshells were compared. As displayed in Figure 4, ^{64}Cu-nanoshell tumor accumulation at one hour after intravenous injection was insignificant, but increased over time. The slowly increased tumor uptake was due to slow removal of ^{64}Cu-nanoshells from the blood pool, as denoted by heart activity on the one-hour image and the pharmacokinetic data depicted in Figure 2B. However, the amount of particles in tumor was much lower compared with the rat with intratumoral injection at any time point. Correspondingly, signals on the liver and spleen were much higher for the intravenously injected rat than the intratumorally injected one at all time points, especially at 44 hours post-injection. These results agree with each other and indicate significant uptake of intravenously injected gold nanoshells by the reticuloendothelial system, suggesting that intratumoral injection was a better administration route to provide a high concentration of gold nanoshells at tumor site and low accumulation in the organs of the reticuloendothelial system.

Biodistribution

All the rats were sacrificed at 46 hours post-injection, and major organs were collected. The amount of ^{64}Cu-DOTA, ^{64}Cu-DOTA-PEG, and ^{64}Cu-nanoshells in the tissue samples

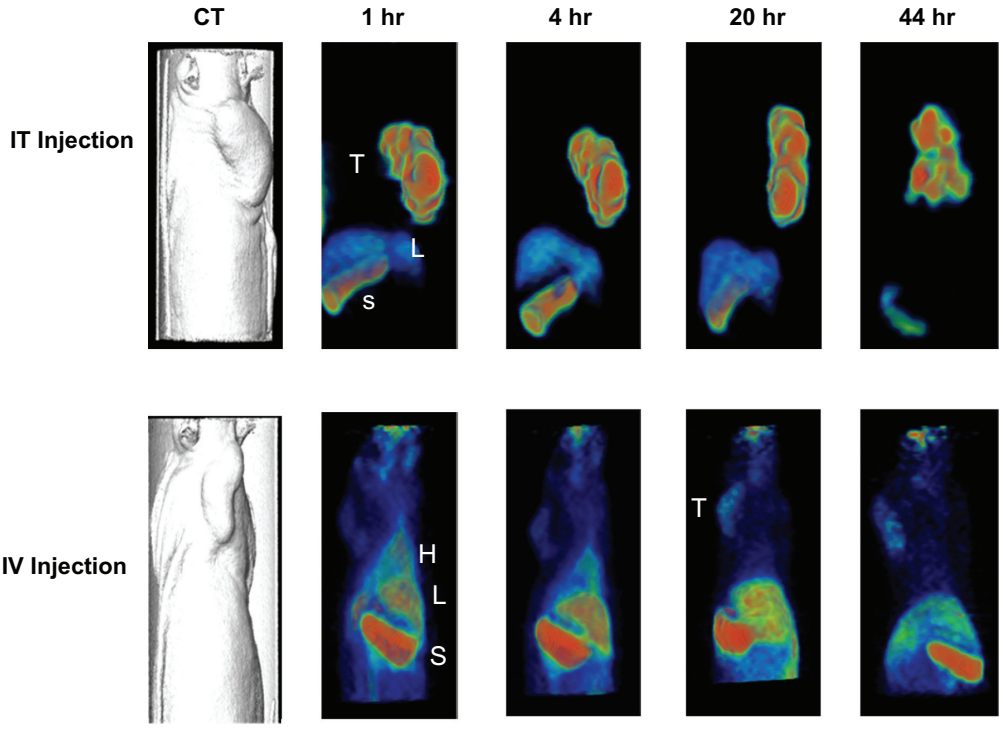

Figure 4 Positron emission tomographic images of two head and neck squamous cell carcinoma xenograft-bearing nude rats acquired at various time points after intratumoral injection and intravenous injection of ^{64}Cu-nanoshells. For intratumoral injection, gold nanoshell accumulation in tumor remained consistently high during the 44 hours post-injection period; the accumulation in liver and spleen could be observed in the first 20 hours, but became much less at 44 hours. For intravenous injection, gold nanoshell accumulation in tumor was much less compared with intratumoral injection throughout the 44 hours; the highest amount of gold nanoshells were found in the spleen and liver.

Notes: Surface-rendered CT images depicting tumor location are also shown. Color intensity scale is denoted as red > yellow > green > blue.

Abbreviations: H, heart; L, liver; S, spleen; T, tumor; CT, computed tomography; IT, intratumoral; IV, intravenous.

was quantified by gamma well counter. The percentages of injected dose (all given by intratumoral injection) per gram of tissue and per organ were calculated and shown in Table 1. Statistical analysis was performed to compare the differences in tissue uptake between the two controls and the ^{64}Cu-nanoshells. As we can see, accumulation of the ^{64}Cu-nanoshells in the tumor, spleen, liver, and urine (0–20 hours) was significantly different from that of the two controls ($P < 0.05$). For the ^{64}Cu-nanoshells, the highest %ID was located in the tumor (31.12% ID/organ) followed by the liver, a reticuloendothelial system organ (13.91% ID/organ). It seems that after intratumoral administration, a small percentage of the ^{64}Cu-nanoshells was rapidly taken up by the spleen and liver, and then slowly cleared through the intestine, as evident from the 7.27% ID found in feces at 46 hours post-injection. In contrast, ^{64}Cu-DOTA and ^{64}Cu-DOTA-PEG were rapidly taken up by the liver and kidneys, and then quickly eliminated as feces and urine. Urine samples collected at 0–20 hours post-injection showed much higher radioactivity in rats injected with ^{64}Cu-DOTA and ^{64}Cu-DOTA-PEG than in rats injected with ^{64}Cu-nanoshells (30.63% ID per organ and 18.35% ID per organ versus 0.98% ID per organ). These results match the PET imaging observations as discussed above, and also follow a trend similar to that of the data for intravenous injection of ^{64}Cu-DOTA, ^{64}Cu-DOTA-PEG, and ^{64}Cu-nanoshells, which we have reported previously.[7] They demonstrate that elimination of the two controls happened at an early stage (before 20 hours post-injection), and confirm that the radioisotope was not cleaved from the gold nanoshells and that the biodistribution data for the ^{64}Cu-nanoshells truly reflected their location. They also demonstrate that the elimination patterns for the controls with intratumoral injection and intravenous injection were similar.[7]

We also compared the distribution of ^{64}Cu-nanoshells at the tumor site and other tissues of animals treated with intratumoral and intravenous injection. Figure 4 shows that, with intravenous injection, a higher %ID per gram of tissue was detected in the spleen, liver, and feces, followed by the kidney and tumor; the higher %ID per organ was found in, eg, the liver, feces, and muscle, whereas tumor uptake was very limited. However, with intratumoral injection, the highest %ID per gram of tissue was observed in the spleen, followed by tumor; the highest %ID per organ was found

Table 1 Biodistribution data of ^{64}Cu-DOTA, ^{64}Cu-DOTA-PEG, and ^{64}Cu-NS in HNSCC xenograft-bearing nude rats (n = 3, n = 3, and n = 4) at 46 hours after intratumoral administration

Organ	^{64}Cu-DOTA		^{64}Cu-DOTA-PEG		^{64}Cu-NS	
	%ID/g	%ID/organ	%ID/g	%ID/organ	%ID/g	%ID/organ
Tumor	1.64 ± 1.02	6.90 ± 3.01	1.34 ± 0.43	5.49 ± 1.22	6.28 ± 1.68*	31.12 ± 6.63*
Spleen	0.10 ± 0.01	0.05 ± 0.00	0.17 ± 0.02	0.08 ± 0.01	11.63 ± 9.69	3.50 ± 2.16*
Liver	0.26 ± 0.02	2.67 ± 0.27	0.52 ± 0.10	4.33 ± 0.51	1.34 ± 0.29*	13.91 ± 4.72*
Lung	0.09 ± 0.01	0.09 ± 0.01	0.14 ± 0.03	0.13 ± 0.04	0.17 ± 0.04	0.17 ± 0.06
Kidney	0.39 ± 0.02	0.71 ± 0.10	0.59 ± 0.07	0.97 ± 0.08	0.53 ± 0.13	0.79 ± 0.18
Blood	0.09 ± 0.01	0.98 ± 0.05	0.13 ± 0.02	1.31 ± 0.12	0.16 ± 0.03	1.77 ± 0.35
Skin	0.08 ± 0.01	2.00 ± 0.02	0.13 ± 0.03	3.09 ± 0.57	0.11 ± 0.03	3.01 ± 0.77
Muscle	0.02 ± 0.00	1.99 ± 0.15	0.04 ± 0.01	3.21 ± 0.33	0.04 ± 0.01	3.67 ± 0.86
Bone	0.06 ± 0.01	1.14 ± 0.12	0.08 ± 0.01	1.57 ± 0.20	0.12 ± 0.05	2.40 ± 0.87
Heart	0.10 ± 0.01	0.07 ± 0.00	0.15 ± 0.01	0.09 ± 0.01	0.18 ± 0.05	0.11 ± 0.03
Stomach	0.07 ± 0.02	0.23 ± 0.13	0.13 ± 0.02	0.35 ± 0.27	0.05 ± 0.02	0.26 ± 0.09
Intestine	0.11 ± 0.03	1.31 ± 0.21	0.25 ± 0.07	2.44 ± 0.63	0.21 ± 0.03	2.01 ± 0.45
Cecum	0.14 ± 0.04	0.75 ± 0.34	0.31 ± 0.07	1.60 ± 0.62	0.23 ± 0.05	1.44 ± 0.53
Bladder	0.04 ± 0.02	0.02 ± 0.01	0.09 ± 0.02	0.06 ± 0.02	0.10 ± 0.04	0.06 ± 0.06
Testis	0.08 ± 0.01	0.21 ± 0.04	0.13 ± 0.02	0.29 ± 0.04	0.13 ± 0.03	0.27 ± 0.06
Brain	0.01 ± 0.00	0.02 ± 0.00	0.02 ± 0.00	0.03 ± 0.00	0.02 ± 0.00	0.03 ± 0.01
Urine 0–20 hours	4.34 ± 1.82	30.63 ± 1.78	5.08 ± 3.22	18.35 ± 5.89	0.15 ± 0.11*	0.98 ± 0.66*
Urine 20–42 hours	0.16 ± 0.11	0.63 ± 0.15	0.32 ± 0.22	0.97 ± 0.40	0.16 ± 0.11	0.72 ± 0.49
Feces	1.71 ± 0.42	10.40 ± 2.38	2.85 ± 1.41	18.17 ± 6.80	1.04 ± 0.43	7.27 ± 1.17

Notes: Data are presented as the average ± standard deviation of 3–4 animals per experimental group as percentage injected dose per gram of tissue (%ID/g) and percentage injected dose per organ (%ID/organ). *$P < 0.05$.
Abbreviations: NS, nanoshells; DOTA, 1,4,7,10-tetraazaciclododecane-1,4,7,10-tetraacetic acid; PEG, polyethylene glycol; HNSCC, head and neck squamous cell carcinoma.

in tumor, followed by the liver. These results show that, compared with intravenous injection, intratumoral injection significantly increased the total amount of gold nanoshells in the tumor, as well as the amount of gold nanoshells retained in the tumor even at 46 hours post-injection (0.77% ID/g of tissue versus 6.28% ID/g of tissue, 0.97% ID/organ versus 31.12% ID/organ, $P < 0.001$ for both). In addition, intratumoral injection also decreased the amount of gold nanoshells in healthy tissue, and the differences were significant for most tissues (Figure 5, $P < 0.05$). These findings suggest that intratumoral injection is a better route of nanoparticle administration that significantly improves nanoparticle accumulation at the tumor site and therefore can potentially enhance the efficacy of subsequent photothermal ablation therapy.

Discussion

Several significant barriers exist in solid tumors, such as a stiff extracellular matrix and elevated interstitial fluid pressure,[15,37] which greatly impede penetration and distribution of therapeutics throughout the tumor mass. Direct intratumoral drug administration can not only bypass the major obstacles to systemic delivery, but can also take advantage of those barriers to prevent rapid drug clearance and promote local retention of therapeutic agents. Therefore, this approach has been evaluated relatively extensively for improving the therapeutic effectiveness of many anticancer agents. Moreover, the feasibility of directly injecting tumors has been greatly enhanced recently by advances in imaging technology, which permit the use of image-guided intervention systems. These image-guided systems make it possible to introduce therapeutic agents into areas once believed to be inaccessible without unacceptable risks. However, systematic studies on intratumoral injection of metal nanoparticles suitable for photothermal ablation have rarely been reported, according to our knowledge.

In recent years, nanoparticles have been broadly explored as promising therapeutic and imaging agents. The emergence of noble metal nanostructures with unique photophysical properties has significantly contributed to the development of cancer photothermal therapy. Up to now, gold nanospheres, gold nanorods, gold nanoshells, gold nanocages, and carbon nanotubes have demonstrated photothermal effects due to their strongly enhanced absorption in the visible and near-infrared regions.[38] The focus has been mainly on solid gold nanospheres (under 100 nm in diameter) coupled with visible lasers and gold nanorods (under 100 nm in diameter), and gold nanoshells (100–200 nm in diameter) coupled with near-infrared lasers.[38] The absorption spectra of solid nanospheres,

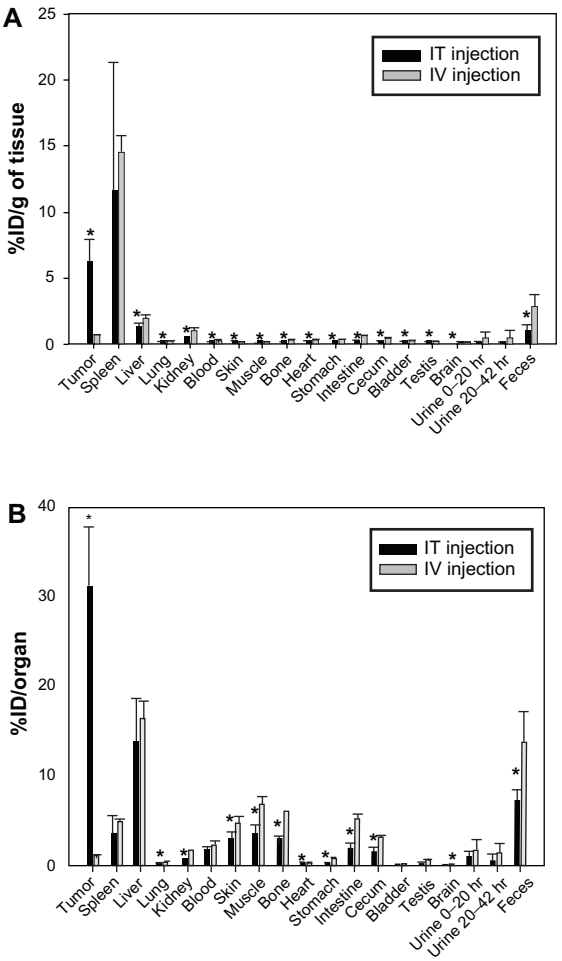

Figure 5 Quantification of the biodistribution of the tumors and organs of head and neck squamous cell carcinoma xenograft-bearing nude rats administered ^{64}Cu-nanoshells by intratumoral injection and intravenous injection at 46 hours post-injection. Values represent the average ± standard deviation of four animals per experimental group. (**A**) percentage injected dose per gram of tissue (%ID/gram of tissue), and (**B**) percentage injected dose per organ (%ID/organ).
Note: *$P < 0.05$ for intratumoral versus intravenous injection.
Abbreviations: IT, intratumoral; IV, intravenous.

nanorods, and nanoshells are sensitive to the size, length/width ratio, and core/shell ratio, respectively. On the other hand, an ideal nanoparticle size for tumor accumulation via the enhanced permeability and retention effect is generally considered to be in the range of 10–100 nm, with the upper limit not well defined.[39] Larger particles (220 nm and above) are generally cleared faster from the blood by the liver (Kupffer cells). Zhang et al reported that ^{111}In-labeled PEG 5000-thioctic acid-coated gold nanospheres with a diameter of 20, 40, and 80 nm had average blood clearance half-lives in mice of 22.5 hours, 10.1 hours, and 15.8 hours, respectively.[36] Von Maltzahn et al reported that their PEG 5000-gold nanorods (approximately 13 × 47 nm) had a 17-hour blood circulation half-life in mice.[30] Our gold nanoshells (with a PEG coating) had an average blood clearance half life of 12.76 hours in tumor-bearing rats,[40] which is similar to gold nanopheres and gold nanorods of smaller sizes. Therefore, their accumulation in tumor tissue should also be similar.

Among the three nanostructures, gold nanoshells have demonstrated effectiveness in photothermal ablation of solid tumors in animal models,[1,2] and are currently under clinical trial for head and neck cancer with an approved investigational device exemption. In connection with the investigational device exemption filing, the Good Laboratory Practices preclinical and laboratory studies did not find any systemic toxicity associated with infusion of the particles into the bloodstream. Based on this evidence, it can be concluded that gold nanoshells are biocompatible and nontoxic. Previously, we have reported the pharmacokinetics and biodistribution of radiolabeled gold nanoshells and their two controls that were intravenously injected into nude rats with HNSCC tumor xenografts. We found that the accumulation of gold nanoshells in tumor tissue through enhanced permeability and retention effect was very limited and the majority of the gold nanoshells were recognized by the reticuloendothelial system and cleared rapidly from the liver and spleen.[6,7] Targeted delivery using targeting moieties such as antibodies, peptides, and small molecules has been extensively studied in order to improve nanoparticle concentration at the tumor site.[37,41–44] We have performed targeted delivery of gold nanoshells and with RGD peptides specific for integrin binding.[5] However, accumulation of gold nanoshells only increased slightly at 20 hours after intravenous injection and no obvious difference was observed at 44 hours, which was much less than we anticipated. In addition, Huang et al re-examined active and passive tumor targeting using gold nanorods and they also found active molecular targeting of the tumor microenvironment did not significantly influence tumor nanoparticle uptake.[31] Therefore, an alternative administration method, intratumoral injection, was investigated in order to increase tumor accumulation of gold nanoshells while decreasing their amount in healthy tissue.

Solid tumors are dense tissues with relatively little interstitial space. The number of injections, volume, and even rate of injection are all factors that contribute to the initial gold nanoshell distribution when given intratumorally. In our studies, we applied techniques that had been evaluated previously for intratumoral delivery of other nanoparticles[14] to ensure good tumor coverage. Each rat received a series of three percutaneous injections (10% of total tumor volume with each injection) slowly (0.5 mL/minute) with a 15-minute gap between each consecutive injection. The needle placements for each injection were equally spaced

along the largest central section area of the tumor, with each needle tip at approximately one-third depth in the tumor along the needle insertion direction. In addition, dense extracellular matrix and the close proximity of cells to one another may be considered amongst the most prominent physical barriers that limit the movement of the relatively large particles, therefore the nanoshell spread within solid tumor may be limited and may rarely extend significantly beyond the site of injection.[45] One of the practical challenges in using an intratumoral injection to perform photothermal cancer therapy is to ensure that the injected nanoparticles evenly distribute throughout the whole tumor so that all of the cancerous cells can be killed by heat generated from the adjacent particles. Use of high-resolution imaging techniques, such as PET and SPECT, can provide detailed intratumoral distribution information using a radiolabeled agent. In addition, noninvasive imaging techniques may also be important tools for the planning of proposed intratumoral injection procedures and for monitoring thermal ablation laser treatment. Our studies in HNSCC tumors showed that ^{64}Cu-nanoshells had broad intratumoral diffusion, which would clearly be beneficial in providing uniformly dispersed gold nanoshells throughout the tumor.

The same strategy can also be applied to other popular photothermal agents, such as gold nanorods. Dickerson et al reported plasmonic photothermal treatment of deep tissue malignancies using gold nanorods that were intratumorally and intravenously injected into nu/nu mice. They observed a 2.18-fold higher concentration of nanorods at the tumor sites for the intratumorally injected mice at 2 minutes and a dramatic size decrease in squamous cell carcinoma xenografts for intratumoral ($P < 0.0001$) and intravenous ($P < 0.0008$) administration in the treated mice.[46] Further photothermal treatment will be undertaken in animals that are intratumorally infused with gold nanoshells for comparison of the therapeutic effectiveness with traditional intravenous injection. A better assessment of intratumoral administration should provide future guidance on current cancer therapy.

Acknowledgments

This work was performed under funding from Nanospectra Biosciences Inc, through NIST ATP Cooperative Agreement Number 70NANB4H3040. We thank the Pharmaceutical Research and Manufacturers of America Foundation and NIH/RTRN grant (5U54RR022762-05) to support the work of HX.

Disclosure

The authors report no conflicts of interest in this work.

References

1. Hirsch LR, Stafford RJ, Bankson, JA, et al. Nanoshell-mediated near-infrared thermal therapy of tumors under magnetic resonance guidance. *Proc Natl Acad Sci U S A*. 2003;100:13549–14554.
2. O'Neal DP, Hirsch LR, Halas NJ, Payne JD, West JL. Photo-thermal tumor ablation in mice using near-infrared-absorbing nanoparticles. *Cancer Lett*. 2004;209:171–176.
3. Oldenberg SJ, Averitt RD, Westcott SL, Halas NJ. Nanoengineering of optical resonances. *Chem Phys Lett*. 1998;28:243–247.
4. Maeda H, Fang J, Inutsuka T, Kitamoto Y. Vascular permeability enhancement in solid tumor: various factors, mechanisms involved and its implications. *Int Immunopharmacol*. 2003;3:319–328.
5. Xie H, Diagaradjane P, Deorukhkar AA, et al. Integrin αvβ3-targeted gold nanoshells augment tumor vasculature-specific imaging and therapy. *Int J Nanomedicine*. 2011;6:259–269.
6. Xie H, Wang Z, Bao A, Goins B, Phillips WT. Radiolabeled gold nanoshells for in vivo imaging: example of methodology for initial evaluation of biodistribution of a novel nanoparticle. In: Hackensack NJ, editor. *Nanoimaging – Biomedical Nanotechnology*. Pan Stanford Publishing Pte Ltd; 2011.
7. Xie H, Wang ZJ, Bao A, Goins B, Phillips WT. In vivo PET imaging and biodistribution of radiolabeled gold nanoshells in rats with tumor xenografts. *Int J Pharm*. 2010;395:324–330.
8. Goldberg EP, Hadba AR, Almond BA, Marotta JS. Intratumoral cancer chemotherapy and immunotherapy: opportunities for non-systemic preoperative drug delivery. *J Pharm Pharmacol*. 2002;54:159–180.
9. Brincker H. Direct intratumoral chemotherapy. *Crit Rev Oncol Hematol*. 1993;15:91–98.
10. Walter KA, Tamargo RJ, Olivi A, Burger PC, Brem H. Intratumoral chemotherapy. *Neurosurgery*. 1995;37:1128–1145.
11. Nomura T, Nakajima S, Kawabata K, Yamashita F, Takakura Y, Hashida M. Intratumoral pharmacokinetics and in vivo gene expression of naked plasmid DNA and its cationic liposome complexes after direct gene transfer. *Cancer Res*. 1997;57:2681–2686.
12. Duvillard C, Romanet P, Cosmidis A, Beaudouin N, Chauffert B. Phase 2 study of intratumoral cisplatin and epinephrine treatment for locally recurrent head and neck tumors. *Ann Otol Rhinol Laryngol*. 2004;113:229–233.
13. Lammers T, Peschke P, Kuhnlein R, et al. Effect of intratumoral injection on the biodistribution and the therapeutic potential of HPMA copolymer-based drug delivery systems. *Neoplasia*. 2006;8:788–795.
14. Bao A, Phillips WT, Goins B, et al. Potential use of drug carried-liposomes for cancer therapy via direct intratumoral injection. *Int J Pharm*. 2006;316:162–169.
15. French JT, Goins B, Saenz M, et al. Interventional therapy of head and neck cancer with lipid nanoparticle-carried rhenium 186 radionuclide. *J Vasc Interv Radiol*. 2010;21:1271–1279.
16. Gultepe E, Reynoso FJ, Jhaveri A, et al. Monitoring of magnetic targeting to tumor vasculature through MRI and biodistribution. *Nanomedicine (Lond)*. 2010;5:1173–1182.
17. Al-Ghananeem AM, Malkawi AH, Muammer YM, et al. Intratumoral delivery of paclitaxel in solid tumor from biodegradable hyaluronan nanoparticle formulations. *AAPS Pharm Sci Tech*. 2009;10:410–417.
18. Li X, Li R, Qian X, et al. Superior antitumor efficiency of cisplatin-loaded nanoparticles by intratumoral delivery with decreased tumor metabolism rate. *Eur J Pharm Biopharm*. 2008;70:726–734.
19. Hamoudeh M, Fessi H, Salim H, Barbos D. Paclitaxel-loaded microparticles for intratumoral administration via the TMT technique: preparation, characterization, and preliminary antitumoral evaluation. *Drug Dev Ind Pharm*. 2008;34:796–806.
20. Zheng D, Li D, Lu X, Feng Z. Enhanced antitumor efficiency of docetaxel-loaded nanoparticles in a human ovarian xenograft model with lower systemic toxicities by intratumoral delivery. *Oncol Rep*. 2010;23:717–724.

21. Ghosh S, Dutta S, Gomes E, et al. Increased heating efficiency and selective thermal ablation of malignant tissue with DNA-encased multiwalled carbon nanotube. *ACS Nano*. 2009;3:2667–2673.
22. Khan MK, Minc LD, Nigavekar SS, et al. Fabrication of {198Au0} radioactive composite nanodevices and their use for nanobrachytherapy. *Nanomedicine*. 2008;4:57–69.
23. Rossin R, Pan D, Qi K, et al. ^{64}Cu-labeled folate-conjugated shell cross-linked nanoparticles for tumor imaging and radiotherapy: synthesis, radiolabeling, and biologic evaluation. *J Nucl Med*. 2005;46:1210–1218.
24. Chanda N, Kan P, Watkinson LD, et al. Radioactive gold nanoparticles in cancer therapy: therapeutic efficacy studies of GA-198 AuNP nanoconstruct in prostate tumor-bearing mice. *Nanomedicine*. 2010;6:201–209.
25. Lee JE, Lee N, Kim T, Kim J, Hyeon T. Multifunctional mesoporous silica nanocomposite nanoparticles for theranostic applications. *Acc Chem Res*. 2011;44:893–902.
26. Becker AL, Johnston AP, Caruso F. Layer-by-layer-assembled capsules and films for therapeutic delivery. *Small*. 2010;6:1836–1852.
27. Ariga K, Lvov YM, Kawakami K, Ji Q, Hill JP. Layer-by-layer self-assembled shells for drug delivery. *Adv Drug Deliv Rev*. 2011;63:762–771.
28. Ariga K, McShane M, Lvov YM, Ji Q, Hill JP. Layer-by-layer assembly for drug delivery and related applications. *Expert Opin Drug Deliv*. 2011;8:633–644.
29. Rosenthal SJ, Chang JC, Kovtun O, McBride JR, Tomlinson ID. Biocompatible quantum dots for biological applications. *Chem Biol*. 2011;18:10–24.
30. von Maltzahn G, Park JH. Agrawal A, et al. Computationally guided photothermal tumor therapy using long-circulating gold nanorod antennas. *Cancer Res*. 2009;69:3892–3900.
31. Huang X, Peng X, Wang Y, Shin DM, El-Sayed MA, Nie S. A reexamination of active and passive tumor targeting by using rod-shaped gold nanocrystals and covalently conjugated peptide ligands. *ACS Nano*. 2010;4:5887–5896.
32. Oldenburg SJ, Jackson JB, Westcott SL, Halas NJ. Infrared extinction properties of gold nanoshells. *Appl Phys Lett*. 1999;111:2897–2899.
33. Bao A, Phillips WT, Goins B, et al. Setup and characterization of a human head and neck squamous cell carcinoma xenograft model in nude rats. *Otolaryngol Head Neck Surg*. 2006;135:853–857.
34. Frank D. Physiological data of laboratory animals. In: Melby EJ, Altman N, editors. *Handbook of Laboratory Animal Science*. Boca Raton, FL: CRC Press; 1976.
35. Petty C. *Research Techniques in the Rat*. Springfield, IL: Charles C Thomas; 1982.
36. Zhang G, Yang Z, Lu W, et al. Influence of anchoring ligands and particle size on the colloidal stability and in vivo biodistribution of polyethylene glycol-coated gold nanoparticles in tumor-xenografted mice. *Biomaterials*. 2009;30:1928–1936.
37. Holback H, Yeo Y. Intratumoral drug delivery with nanoparticulate carriers. *Pharm Res*. 2011;28:1819–1830.
38. Huang X, Jain PK, El-Sayed IH, El-Sayed MA. Plasmonic photothermal therapy (PPTT) using gold nanoparticles. *Lasers Med Sci*. 2008;23:217–228.
39. Davis ME, Chen ZG, Shin DM. Nanoparticle therapeutics: an emerging treatment modality for cancer. *Nat Rev Drug Discov*. 2008;7:771–782.
40. Xie H, Gill-Sharp KL, O'Neal DP. Quantitative estimation of gold nanoshell concentrations in whole blood using dynamic light scattering. *Nanomedicine*. 2007;3:89–94.
41. Eghtedari M, Liopo AV, Copland JA, Oraevsky AA, Motamedi M. Engineering of hetero-functional gold nanorods for the in vivo molecular targeting of breast cancer cells. *Nano Lett*. 2008;9:287–291.
42. El-Sayed IH, Huang X, El-Sayed MA. Selective laser photo-thermal therapy of epithelial carcinoma using anti-EGFR antibody conjugated gold nanoparticles. *Cancer Lett*. 2006;239;129–135.
43. Huang YF, Chang HT, Tan W. Cancer cell targeting using multiple aptamers conjugated on nanorods. *Anal Chem*. 2008;80:567–572.
44. Mann AP, Bhavane RC, Somasunderam A, et al. Thioaptamer conjugated liposomes for tumor vasculature targeting. *Oncotarget*. 2011;2:298–304.
45. Smith E, Breznik J, Lichty BD. Strategies to enhance viral penetration of solid tumors. *Hum Gene Ther*. 2011;22:1053–1060.
46. Dickerson EB, Dreaden EC, Huang X, et al. Gold nanorod assisted near-infrared plasmonic photothermal therapy (PPTT) of squamous cell carcinoma in mice. *Cancer Lett*. 2008;269:57–66.